The methyltransferase adaptor protein Trm112 is involved in biogenesis of both ribosomal subunits

Richa Sardana and Arlen W. Johnson
Section of Molecular Genetics and Microbiology and Institute for Cellular and Molecular Biology, The University of Texas at Austin, Austin, TX 78712

ABSTRACT **We previously identified Bud23 as the methyltransferase that methylates G1575 of rRNA in the P-site of the small (40S) ribosomal subunit. In this paper, we show that Bud23 requires the methyltransferase adaptor protein Trm112 for stability in vivo. Deletion of Trm112 results in a *bud23*Δ-like mutant phenotype. Thus Trm112 is required for efficient small-subunit biogenesis. Genetic analysis suggests the slow growth of a *trm112*Δ mutant is due primarily to the loss of Bud23. Surprisingly, suppression of the *bud23*Δ-dependent 40S defect revealed a large (60S) biogenesis defect in a *trm112*Δ mutant. Using sucrose gradient sedimentation analysis and coimmunoprecipitation, we show that Trm112 is also involved in 60S subunit biogenesis. The 60S defect may be dependent on Nop2 and Rcm1, two additional Trm112 interactors that we identify. Our work extends the known range of Trm112 function from modification of tRNAs and translation factors to both ribosomal subunits, showing that its effects span all aspects of the translation machinery. Although Trm112 is required for Bud23 stability, our results suggest that Trm112 is not maintained in a stable complex with Bud23. We suggest that Trm112 stabilizes its free methyltransferase partners not engaged with substrate and/or helps to deliver its methyltransferase partners to their substrates.**

Monitoring Editor
A. Gregory Matera
University of North Carolina

Received: May 14, 2012
Revised: Jul 23, 2012
Accepted: Aug 30, 2012

INTRODUCTION

RNA plays a pivotal role in many cellular processes. The regulation of synthesis, folding, and processing of the RNA species is therefore integral to regulation of cellular functions. Posttranscriptional modifications during the processing of nascent precursor RNA transcripts have long been suggested to be mechanisms that modulate RNA function or stability and influence gene expression (Helm, 2006). RNA methylation is one such commonly observed modification and has been reported in rRNA, tRNA, mRNA, small nuclear RNA, small nucleolar RNA (snoRNA), tmRNA, and micro RNA, as well as viral RNA. Methylation of RNA can occur at different positions of the nitrogenous base as well as at the ribose sugar.

rRNAs are subjected to several posttranscriptional modifications, in particular base methylations, 2′-*O*-ribose methylations, and pseudouridylations. Most of these modifications are localized in the functionally important centers of the ribosome—the peptidyltransferase center and the decoding center (Decatur and Fournier, 2002). However, a large percentage of these rRNA modifications are not essential individually and are thought to fine-tune the efficiency and accuracy of the translation process. While the majority of rRNA modifications are 2′-*O*-ribose methylations and pseudouridylations, targeted by C/D-box snoRNAs and H/ACA-box snoRNAs using common modification enzymes, base methylations are typically catalyzed by specific *S*-adenosylmethionine (SAM)-dependent methyltransferases (Henras *et al.*, 2008).

Small-subunit (40S) 18S rRNA in *Saccharomyces cerevisiae* contains only three base methylations. Two of these, at positions A1781 and A1782, are catalyzed by Dim1 (Lafontaine *et al.*, 1994). Dim1 is essential for viability, but the methylations catalyzed by it are not

This article was published online ahead of print in MBoC in Press (http://www.molbiolcell.org/cgi/doi/10.1091/mbc.E12-05-0370) on September 5, 2012.

Address correspondence to: Arlen Johnson (arlen@austin.utexas.edu).

Abbreviations used: GFP, green fluorescent protein; HA, hemagglutinin; IgG, immunoglobulin G; IP, immunoprecipitation; PMSF, phenylmethylsulfonyl fluoride; SAM, *S*-adenosylmethionine; snoRNA, small nucleolar RNA; TAP, tandem affinity purification; TCA, trichloroacetic acid; TEV protease, tobacco etch virus protease; YPD, yeast–peptone–dextrose.

(Lafontaine *et al.*, 1995). The third base methylation, at position G1575, is catalyzed by Bud23 (White *et al.*, 2008). The methylated guanosine is located in the P-site of the small subunit, and its methylation is conserved throughout eukaryotes. However, similar to Dim1 and despite its seemingly important location, methylation of G1575 is also not essential (White *et al.*, 2008). Large-subunit (60S) 25S rRNA contains at least six base methylations (Piekna-Przybylska *et al.*, 2007), but none of the methyltransferases responsible for these modifications has been characterized.

Transfer RNAs also undergo a large variety of modifications, including several base methylations. Methyltransferases responsible for several of these methylations have been identified (Dunin-Horkawicz *et al.*, 2006). Interestingly, at least two of the SAM-dependent tRNA methyltransferases (Trm9 and Trm11) have been shown to interact with the small zinc finger protein Trm112 (Purushothaman *et al.*, 2005; Studte *et al.*, 2008). Additionally, Trm112 has also been shown to be the coactivator of Mtq2, a protein that methylates the translation termination factor, eRF1 (Heurgue-Hamard *et al.*, 2006; Liger *et al.*, 2011). In the case of Mtq2, Trm112 is also required for its stability. The known methyltransferase partners of Trm112 are all of the same family of seven β-strand proteins. Thus Trm112 appears to play a common role in facilitating the function of multiple methyltransferases affecting different aspects of translation.

In this work, we provide evidence that Trm112 also acts in ribosome biogenesis, as a coactivator for Bud23 in 40S biogenesis, and in 60S biogenesis, probably through Nop2 and Rcm1. Our work elucidates a novel role of Trm112 in ribosome biogenesis and extends the function of Trm112 to all aspects of the translation machinery: the two ribosomal subunits, tRNAs, and translation factors.

RESULTS

Bud23 and Trm112 interact in vivo

We had previously identified Bud23 as a methyltransferase involved in the biogenesis of the small (40S) ribosomal subunit (White *et al.*, 2008). To further characterize the function of Bud23, we carried out tandem affinity purification (TAP) to identify interacting partners. In addition to known 40S-associated factors, we identified Trm112 (unpublished data). This interaction was intriguing, because Trm112 has been shown to be a "hub" protein that interacts with at least three methyltransferases affecting different aspects of translation, by modifying tRNAs and a translation factor (Mazauric *et al.*, 2010; Liger *et al.*, 2011). An interaction with Bud23 would implicate Trm112 in ribosome biogenesis as well. We confirmed the physical interaction between Bud23 and Trm112 by two means: coimmunoprecipitation and yeast two-hybrid assay. C-terminally TAP-tagged Bud23 was expressed in a strain containing genomic C-terminally green fluorescent protein (GFP)-tagged Trm112. Total extracts were immunoprecipitated against the TAP tag using immunoglobulin G (IgG) Sepharose and were analyzed for Trm112-GFP by Western blotting using anti-GFP antibody. Rps8 was used as a positive control for Bud23-TAP purification, as Bud23 associates with pre-40S particles. Trm112-GFP was specifically immunoprecipitated with TAP-tagged Bud23 (Figure 1A).

To test two-hybrid interaction, we cloned Trm112 with a C-terminal fusion of Gal4 DNA binding domain in pGBKT7 and Bud23 with an N-terminal fusion of Gal4 activation domain in pACT2. We observed positive two-hybrid interaction between Bud23 and Trm112, as shown by growth on medium lacking histidine (Figure 1B). Thus coimmunoprecipitation and yeast two-hybrid assays confirm the mass spectroscopy result that Bud23

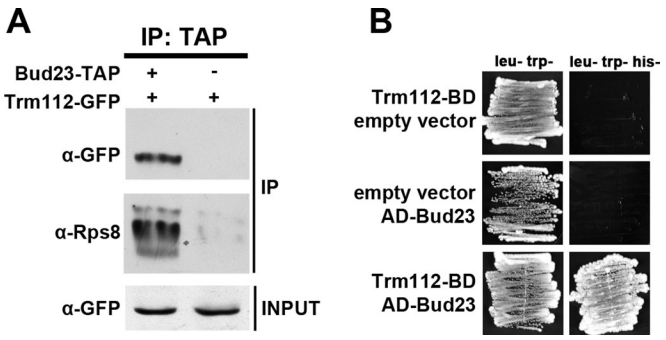

FIGURE 1: Bud23 and Trm112 interact in vivo. (A) Bud23-TAP immunoprecipitates Trm112-GFP. Extracts from cells expressing Trm112-GFP (AJY3446) and Bud23-TAP (pAJ2558) were immunoprecipitated with IgG-Sepharose. Extracts prepared from cells expressing Trm112-GFP and untagged Bud23 were used as negative control. Immunoprecipitated proteins were subjected to SDS–PAGE and Western blotting using anti–GFP-horseradish peroxidase and anti-Rps8 antibodies to detect Trm112-GFP and Rps8, respectively. (B) PJ69-4α strain containing Trm112-Gal4BD (pAJ2895) and Gal4AD-Bud23 (pAJ2768) was patched on Leu-Trp and Leu-Trp-His plates. Corresponding controls containing the corresponding empty vectors were also patched on selective plates to rule out the possibility of self-activation of the HIS3 reporter. Plates were incubated at 30°C for 2 d.

and Trm112 interact in vivo. Although we cannot exclude the possibility that their interaction is bridged by a third protein, Trm112 is known to bind other seven β-strand methyltransferases directly. Thus it is likely that Bud23 binds Trm112 directly. Indeed, while this work was in progress, a direct complex of Bud23 and Trm112 was reported (Figaro *et al.*, 2012).

Bud23 and Trm112 show positive genetic interaction

Proteins involved in the same or related pathways often exhibit genetic interactions. To test for genetic interaction between Bud23 and Trm112, we compared the growth rates of wild-type, *bud23*Δ, and *trm112*Δ single mutants and a *bud23*Δ *trm112*Δ double mutant. Deletion of either *BUD23* or *TRM112* resulted in a severe growth defect (Figure 2A, panels 1–3). However, the double mutant grew at approximately the same rate as the individual single mutants (Figure 2A, panel 4). Quantitative growth rates were determined in liquid cultures. Fitness was calculated as the doubling time of wild-type divided by that of the mutant. If there were no genetic interaction, then the double mutant would be expected to grow with a fitness calculated as the product of the individual fitnesses of the single mutants (Dixon *et al.*, 2009). The *bud23*Δ showed a fitness of 0.30 compared with wild-type, and *trm112*Δ had a fitness of 0.27. For no genetic interaction, the *bud23*Δ *trm112*Δ double mutant would be expected to grow with a fitness of 0.08 (0.30×0.27). However, the double mutant grew with a fitness of 0.29, exhibiting a 72% greater than expected fitness and indicating a strong positive genetic interaction (Figure 2B).

We identified a mutation in UTP14 (A758G) encoding a component of the small-subunit processome as an extragenic suppressor of the growth defect of *bud23*Δ (Figure 2A, panel 5; unpublished data). This mutation in UTP14 also suppressed a *trm112*Δ mutant (Figure 2A, panel 6, and 2B). Furthermore, Utp14-GFP mislocalized from the nucleolus to the nucleoplasm in a *trm112*Δ mutant in a manner similar to that observed in a *bud23*Δ mutant (Figure 2C; unpublished data). This mislocalization can be corrected in both a *bud23*Δ and a *trm112*Δ mutant by the utp14-A758G suppressor.

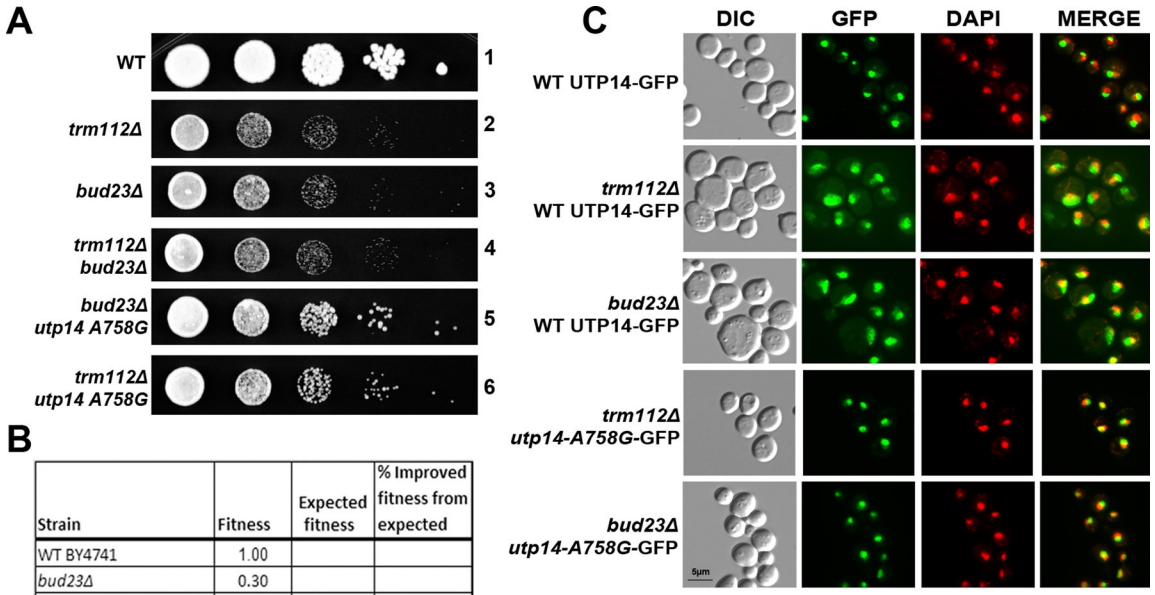

B

Strain	Fitness	Expected fitness	% Improved fitness from expected
WT BY4741	1.00		
bud23Δ	0.30		
trm112Δ	0.27		
trm112Δ bud23Δ	**0.29**	**0.08**	**72**
bud23Δ utp14A758G	0.49	0.30	39
trm112Δ utp14A758G	0.46	0.27	40

FIGURE 2: Bud23 and Trm112 show positive genetic interaction. (A) Tenfold serial dilutions of the isogenic wild-type (BY4741), *trm112*Δ (AJY3517) and *bud23*Δ (AJY2161) single mutants, *trm112*Δ *bud23*Δ (AJY3524) double mutant, and *bud23*Δ *utp14-A758G* (AJY3549) and *trm112*Δ *utp14-A758G* (AJY3547) mutants were spotted on complete rich media (YPD) and incubated at 30°C for 2 d. (B) Quantitation of growth rates of the mutants shown in (A). Strains were grown in 96-well plates in complete rich media (YPD) at 30°C and density-monitored continuously for 36 h. The fitness of each strain was calculated by dividing the doubling time of the isogenic wild-type by that of the mutant. Expected fitness of the double mutants for no genetic interaction was calculated as the product of the observed fitness of the individual mutants. (C) *trm112*Δ and *bud23*Δ mutants show a similar mislocalization of Utp14. Indicated strains expressing genomic wild-type Utp14-GFP or *utp14-A758G*-GFP were grown in synthetic complete media to mid–log phase at 30°C and analyzed for GFP fluorescence. The nuclei were stained with 4′,6-diamidino-2-phenylindole (DAPI; here falsely colored red).

Thus we conclude that Bud23 and Trm112 functionally interact with each other and that the mutants are defective for the same step in 40S ribosome biogenesis.

That *bud23*Δ and *trm112*Δ show strong positive genetic interaction and that the severe growth defect of *trm112*Δ is partially suppressed by a mutation that suppressed *bud23*Δ suggests the bulk of the *trm112*Δ growth defect is contributed by a failure in Bud23 function. This is rather surprising, considering that Trm112 interacts with multiple methyltransferases involved in multiple aspects of translation.

Trm112 is required for 40S and 60S ribosome biogenesis

Polysome profile analysis by sucrose density gradient centrifugation is a sensitive assay for monitoring ribosome biogenesis and translation defects. We used polysome analysis to assay for ribosome biogenesis defects in *trm112*Δ. As reported earlier, a *bud23*Δ mutant exhibited a strong 40S biogenesis defect resulting in a strong subunit imbalance with almost no free 40S, very high free 60S levels, and reduced polysomes (Figure 3A). A *trm112*Δ mutant also exhibited a 40S biogenesis defect; however, the extent of subunit imbalance was less severe than in a *bud23*Δ mutant. We note that the subunit imbalance in this strain is less than what was recently reported for *trm112*Δ (Figaro *et al.*, 2012). However, we observed similar profiles from multiple spore clones after sporulating a trm112 heterozygous diploid (unpublished data), suggesting that this profile specifically reflects loss of *TRM112* in this strain background. We also analyzed *trm112*Δ containing the utp14-A758G suppressor. Surprisingly, this mutant revealed a 60S biogenesis defect as seen by a reversed free-subunit imbalance (free 60S levels lower than 40S) and half-mer polysomes. Half-mers contain 43S initiation complexes that have not yet been joined by 60S subunits and are a common consequence of reduced 60S levels. These results suggest that Trm112 plays a role in both 40S and 60S biogenesis pathways; however, the 40S defect is more pronounced than the 60S biogenesis defect in a *trm112*Δ mutant.

We also compared the effect of deletion of *TRM112* and *BUD23* on rRNA processing. Bud23 is required for efficient cleavage at A2 that gives rise to the 27SA2 intermediate (White *et al.*, 2008; unpublished data). Indeed, both mutants were strongly inhibited for A2 cleavage. Both mutants also showed reduced levels of mature 18S rRNA compared with the wild-type control: *bud23*Δ displayed a 61% reduction and *trm112*Δ a 56% reduction in 18S rRNA when normalized to U2 (Figure 3C). However, we noted that the *trm112*Δ mutant also displayed a 43% reduction in level of 25S rRNA of the 60S subunit (Figure 3, B and C). The simultaneous reduction of both 18S and 25S rRNA in the *trm112*Δ mutant likely accounts for the relatively normal subunit balance seen in the polysome profile of the *trm112*Δ mutant (Figure 3A). The similar 27SA2 cleavage defect suggests that Bud23 and Trm112 have a common function in A2 cleavage. In addition, the reduced 25S levels and the polysome profile analysis suggest that Trm112 is also required for efficient 25S processing.

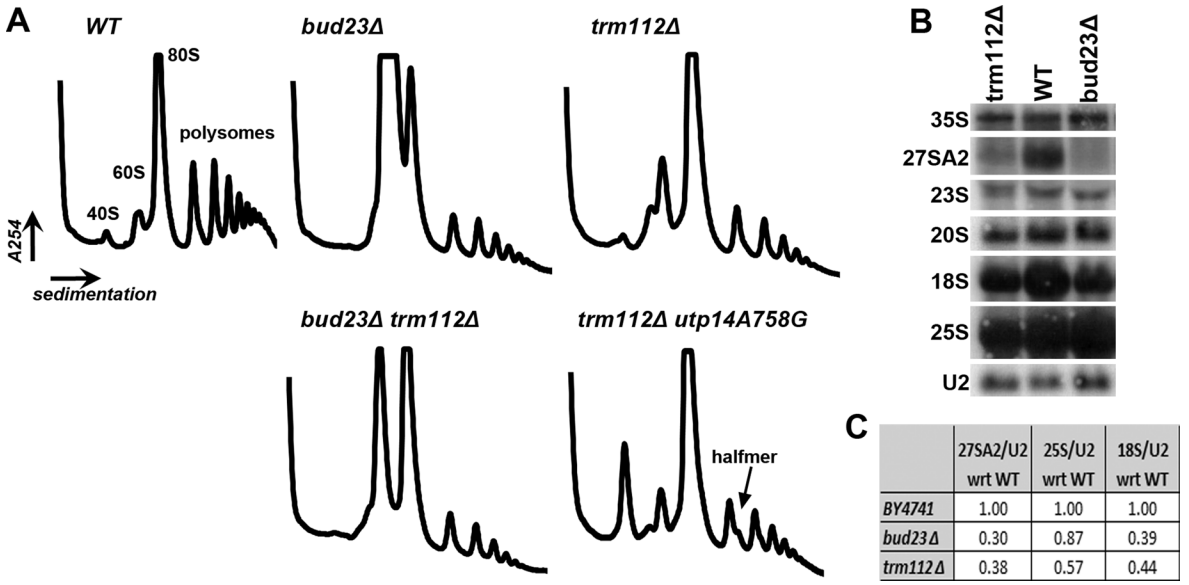

C

	27SA2/U2 wrt WT	25S/U2 wrt WT	18S/U2 wrt WT
BY4741	1.00	1.00	1.00
bud23Δ	0.30	0.87	0.39
trm112Δ	0.38	0.57	0.44

FIGURE 3: Trm112 is required for both 40S and 60S biogenesis. (A) *trm112*Δ mutant displays both small- and large-subunit biogenesis defect. Whole-cell extracts from wild-type control (AJY2643), *bud23*Δ (AJY2161), *trm112*Δ (AJY3517), *trm112*Δ *bud23*Δ (AJY3524), and *trm112*Δ *utp14-A758G* (AJY3547) strains were subjected to sucrose density gradient ultracentrifugation. Absorbance at 254 nm was used to generate polysome profiles. The position of 40S, 60S, and 80S peaks and half-mers is marked. (B) *trm112*Δ mutant exhibits both small- and large-subunit rRNA-processing defect. Total RNA extracted from the indicated strains grown to OD_{600} ~ 0.3 in YPD at 30°C was separated on an agarose/formaldehyde denaturing gel, transferred to a membrane, and probed by hybridization with indicated oligonucleotide probes to identify rRNA-processing intermediates. The oligonucleotide probes used for Northern blotting are listed in Table 3. (C) Quantitation of Northern blots shown in (B). The hybridization signals were detected by phosphorimaging and quantified using Quantity One (Bio-Rad). Signals were normalized to U2 as a loading control, and numbers indicate levels with respect to wild-type (wrt WT).

Sedimentation of Trm112 is not dependent on Bud23

Because of the interaction between Trm112 and Bud23, we examined their sedimentation on sucrose gradients to determine whether they cosediment, which is indicative of a stable complex in vivo. Extracts were prepared from cells expressing TAP-tagged Trm112 and episomally expressed Bud23 and subjected to sucrose density gradient centrifugation. We used two different tagged versions of Bud23, tagged at either the N- or C-terminus. Trm112-TAP sedimented at the position of 60S, whereas N-terminally tagged Bud23 occurred predominantly at the position of 90S, overlapping with the 90S marker Mpp10 (Figure 4, top). A small amount of Trm112 was also present at the top of the gradient. On the other hand, C-terminally tagged Bud23 sedimented at the position of 40S (Figure 4, bottom). Recent work using an antibody against native Bud23-Trm112 complex showed that both proteins cosediment at the position of 80S/90S, suggesting that the two proteins exist in a stable complex (Figaro *et al.*, 2012). Although both tagged versions of Bud23 and Trm112-TAP used in our study are functional, the nature of the tag and/or the end of the protein that is tagged has a strong effect on the sedimentation of the proteins. Nevertheless, the fact that both tagged versions of Bud23 were functional, and neither cosedimented with Trm112-TAP in our experiments, demonstrates that these two proteins do not always coexist in a stable complex, despite the fact that Trm112 is needed for Bud23 stability (see below and Figure 7 later in the paper).

We next explored whether the sedimentation of Trm112 depended on the presence of Bud23. Trm112 was present at the top of the gradient and in the 60S region, regardless of the presence or absence of Bud23 (Figure 5A), indicating that its sedimentation was independent of Bud23. To confirm that Trm112-TAP indeed was sedimenting with 60S, we next ran gradients for Trm112-TAP under dissociative conditions and monitored the sedimentation of Mpp10 as a 90S marker, Nop2 as a pre-60S marker, Rpl10 as a 60S marker, and Rps8 as a 40S marker. Under these conditions, Trm112 cosedimented most closely with Rpl10 and Nop2, at the position of 60S and not at 40S or 90S (Figure 5B). To support the apparent association of Trm112 with pre-60S or 60S subunits, we assayed for the pre-60S rRNAs associated with Trm112. In agreement with the sedimentation analysis, Trm112-TAP efficiently pulled down the 27S and 7S pre-rRNAs, as well as mature 25S rRNA, but not 20S pre-RNA or U3 snoRNA (Figure 6A). The relative enrichment for 27S and 7S was much greater than for 25S, suggesting that Trm112 is predominantly associated with the pre-60S particle. The association of Trm112 with pre-60S or 60S subunits was substantiated by coimmunoprecipitation of the 60S protein Rpl8 (Figure 6B). The coimmunoprecipitation of pre-60S rRNAs with Trm112 is consistent with the sedimentation of Trm112 at the position of 60S and suggests that Trm112 is predominantly associated with a pre-60S species.

Trm112 coimmunoprecipitates the 60S-related methyltransferases Nop2 and Rcm1

The association of Trm112 with the 60S subunits and the requirement for Trm112 in efficient production of 60S (Figures 3 and 4) suggests that Trm112 has additional partners in 60S biogenesis. Because Trm112 has been shown to interact with multiple methyltransferases, we decided to test whether Trm112 interacts with additional known and uncharacterized methyltransferases that have been suggested as playing a role in 60S biogenesis. We tested Rrp8, Ybr141c, Ylr063w, Nop2, Ybr271w, Rcm1, and Spb1 for interaction with Trm112 by coimmunoprecipitation. C-terminally myc-tagged methyltransferase

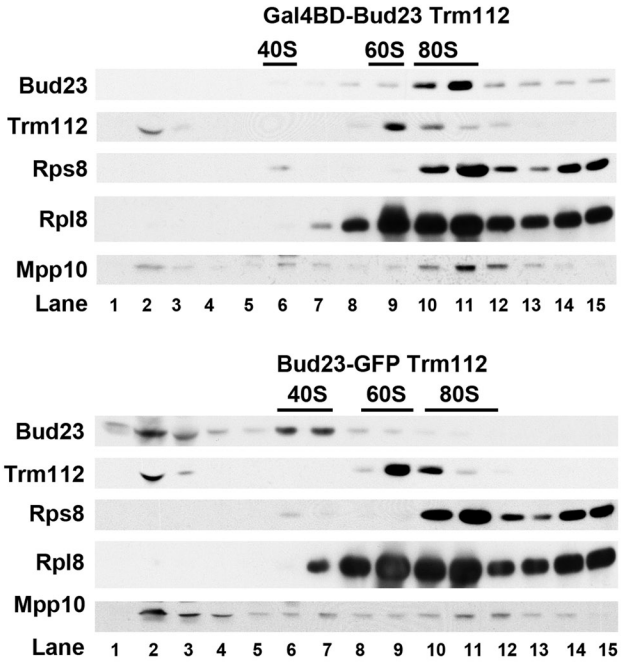

FIGURE 4: Trm112 and Bud23 sediment with different complexes. Whole-cell extracts from cycloheximide-treated AJY3125 expressing genomic Trm112-TAP and the episomal two-hybrid Bud23 construct (N-terminal GAL4BD-myc–tagged Bud23; top) or C-terminal GFP-tagged Bud23 (bottom) were subjected to sucrose density gradient ultracentrifugation. Proteins were precipitated from fractions, subjected to SDS–PAGE, and myc-tagged Bud23, GFP-tagged Bud23, Rps8, Rpl8, and Mpp10 were detected using anti-myc, anti-GFP, anti-Rps8, anti-Rpl8, and anti-Mpp10 antibodies, respectively. TAP tagged Trm112 was detected by its cross-reactivity with anti-Rps8 and anti-Rpl8, as well as with anti-Mpp10 antibodies. The positions of 40S, 60S, and 80S are indicated.

candidates were expressed in a strain containing genomic C-terminally TAP-tagged Trm112. Total extracts were immunoprecipitated against the TAP tag using IgG Sepharose and analyzed for myc-tagged proteins by Western blotting. Trm112-TAP specifically immunoprecipitated two 60S-related methyltransferases, Nop2 and Rcm1 (Figure 6B). Thus coimmunoprecipitation analysis indicates that Trm112 specifically interacts with Nop2 and Rcm1 in vivo.

Trm112 affects the in vivo stability of some, but not all, of its interaction partners

Previous work has shown that interaction with Trm112 solubilizes Mtq2 and Trm9 in *Escherichia coli* extracts (Heurgue-Hamard *et al.*, 2006; Chen *et al.*, 2011). To test the effect of Trm112 on in vivo levels of Bud23, Nop2, and Rcm1, we looked at steady-state levels of these proteins in wild-type and *trm112*Δ mutant cells. We also looked at the levels of Mtq2 and Trm11 as controls for proteins that have previously been characterized as Trm112 interaction partners. Our results show that the absence of Trm112 has a dramatic effect on the in vivo stability of some, but not all, of its interaction partners (Figure 7A). In particular we observed that Bud23 and Mtq2 were strongly reduced in a *trm112*Δ mutant. However the levels of Nop2, Rcm1, and Trm11 were modestly or not at all affected by the absence of Trm112. To further address the effect of Trm112 levels on the steady-state levels of Bud23, we examined Bud23-GFP in a strain expressing Trm112 under control of a galactose-inducible promoter on a plasmid. We then compared the levels of Bud23-GFP in the presence or absence of overexpressed Trm112 (Figure 7B). In the absence of TRM112 overexpression, the levels of Bud23 in saturated cultures were substantially reduced (Figure 7B, compare lanes 2 and 1). This is expected for most factors involved in ribosome biogenesis. However, overexpression of Trm112 resulted in increased levels of Bud23-GFP in growing and in saturated cultures (Figure 7B, compare lanes 3 and 1, and lanes 4 and 2), suggesting that Bud23 levels in cells are dependent, in part, on the level of Trm112.

Specific mutations in Bud23 result in loss of Trm112-Bud23 interaction

We mutated clusters of surface-exposed residues on Bud23 and tested for loss of interaction with Trm112 by two-hybrid assay, as described in Figure 1. The bud23-RSD mutant (R107L, S110A, D112G) resulted in a complete loss of detectable interaction (Figure 8A). We modeled the predicted structure of the methyltransferase domain of Bud23 (White *et al.*, 2008) on the recently described crystal structure of Mtq2-Trm112 (Liger *et al.*, 2011; Figure 8B). Although only R107 is at the interface in the modeled structure, a loop of Trm112 (aa 32–35) is not resolved in the Mtq2-Trm112 structure and thus could interact with additional residues of Bud23. The loss of two-hybrid interaction was not explained by loss of mutant Bud23 protein, as the levels of the Bud23-RSD mutant protein were only slightly diminished compared with wild-type (Figure 8C). However, the two-hybrid construct was a high-copy vector and overexpressed Bud23. Consequently, we switched the bud23-RSD mutant to a low-copy vector to more closely replicate the endogenous expression of Bud23 and assayed its ability to complement a *bud23*Δ mutant. The bud23-RSD mutant was completely nonfunctional in this assay (Figure 8D). In addition, we observed a severe reduction in mutant protein level when expressed from a low-copy vector (Figure 8E), which was similar to that observed for wild-type Bud23 in a *trm112*Δ mutant (Figure 7A). Thus we conclude that specific interaction with Trm112 is critical for the stability, and hence the function, of Bud23 in vivo.

DISCUSSION

Yeast Trm112 is a small 15-kDa zinc finger protein that has been shown to bind to and regulate the catalytic activity and stability of several methyltransferases involved in different aspects of translation (Purushothaman *et al.*, 2005; Heurgue-Hamard *et al.*, 2006; Mazauric *et al.*, 2010; Liger *et al.*, 2011). These include Trm9 and Trm11, which are responsible for methylation of tRNA (Purushothaman *et al.*, 2005; Mazauric *et al.*, 2010), and Mtq2, which is responsible for methylation of the translation termination factor eRF1 (Heurgue-Hamard *et al.*, 2006; Liger *et al.*, 2011). Our work extends the function of Trm112 to biogenesis of both ribosomal subunits through its interaction with the small subunit methyltransferase Bud23 and likely through Nop2 and Rcm1 acting on the large subunit. During the course of this work, a similar function for Trm112 in Bud23 function was reported by Figaro *et al.* (2012).

How does Trm112 affect the function of its methyltransferase partners?

Previously, Trm112 was shown to be required for the solubility of Mtq2 and Trm9 (Heurgue-Hamard *et al.*, 2006; Mazauric *et al.*, 2010). In this study, we show that Trm112 is required for stability of Bud23 in vivo. Despite the fact that Bud23 is required for the highly conserved methylation of G1575 in 18S rRNA, it is the protein and

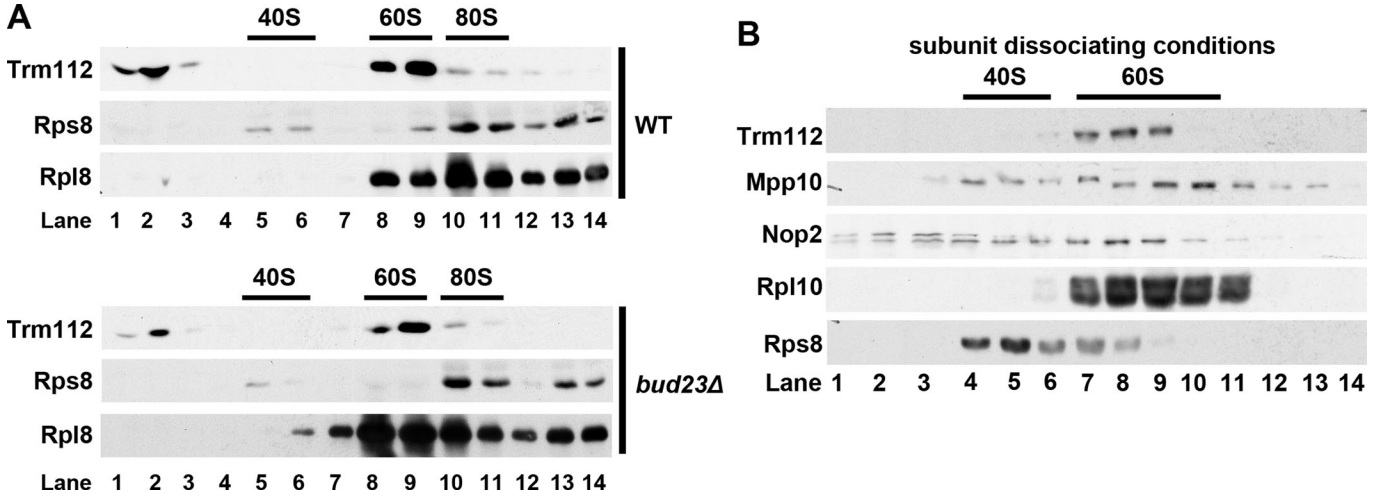

FIGURE 5: Trm112-TAP predominantly sediments with 60S. (A) Sedimentation of Trm112 is not affected by the presence or absence of Bud23. Whole-cell extracts prepared from cycloheximide-treated AJY3560 (Trm112-TAP wild-type Bud23) and AJY3125 (Trm112-TAP *bud23*Δ) were subjected to sucrose density gradient ultracentrifugation. Samples were subjected to SDS–PAGE and Western blotting, as described in Figure 4. (B) Trm112 sediments predominantly at 60S in dissociative gradients. Whole-cell extract from AJY3560 expressing Nop2-13myc (pAJ2895) from a plasmid was prepared under conditions to dissociate ribosomal subunits and fractionated following sucrose density gradient ultracentrifugation. Nop2-13myc and Rpl10 were detected using anti-myc and anti-Rpl10 antibodies, respectively. All the other proteins were detected as described in the legend to Figure 4.

not its methyltransferase activity, per se, that is important for ribosome biogenesis and normal cellular growth (White *et al.*, 2008; Figaro *et al.*, 2012). Bud23 levels are virtually undetectable in the absence of Trm112 and are elevated by the overexpression of Trm112. Figaro *et al.* (2012) showed similar findings and extended this work by demonstrating that the two proteins form a stable complex in vitro and cosediment on sucrose density gradients at the

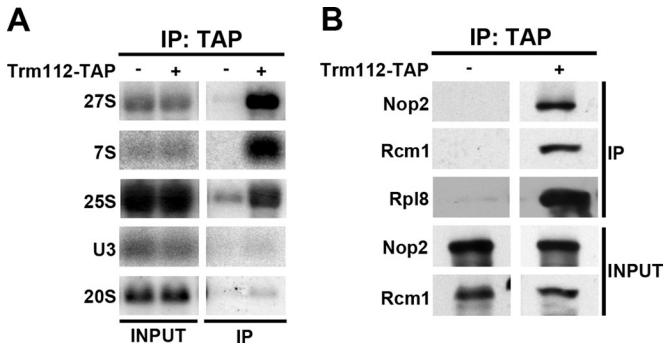

FIGURE 6: Trm112 immunoprecipitates pre-60S RNAs and associated methyltransferases. (A) Trm112-TAP immunoprecipitates 60S-associated pre-rRNAs. Extracts from cells expressing Trm112-TAP (AJY3560) were immunoprecipitated with IgG-Sepharose. Extract prepared from cells expressing untagged Trm112 was used as negative control. Immunoprecipitated RNAs were analyzed for the presence of U3 snoRNA or specific pre- and mature rRNAs by Northern blotting. The oligonucleotide probes used for Northern blotting are listed in Table 3. (B) Trm112-TAP coimmunoprecipitates pre-60S–related methyltransferases, Nop2 and Rcm1. Extracts from cells expressing genomic Trm112-TAP (AJY3560) and plasmid-borne Nop2-13myc (pAJ2875), Rcm1-13myc (pAJ2878), or empty vector were immunoprecipitated with IgG-Sepharose. Immunoprecipitated proteins were subjected to SDS–PAGE and Western blotting using anti-myc and anti-Rpl8 antibodies to detect Nop2-13myc, or Rcm1-13myc and Rpl8, respectively.

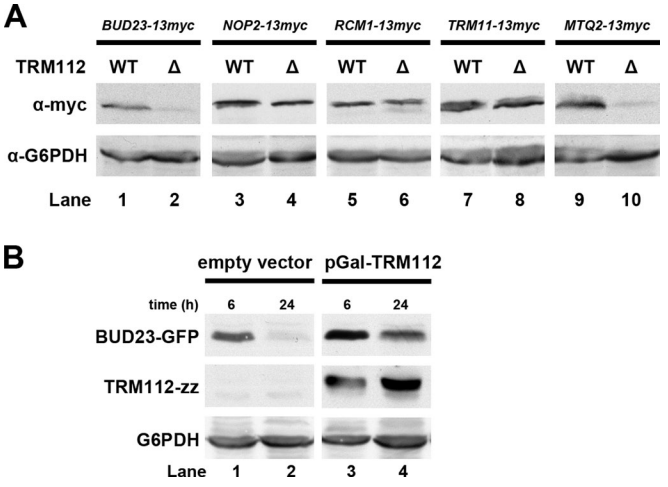

FIGURE 7: Trm112 affects the in vivo stability of some, but not all, interaction partners. (A) Absence of Trm112 affects the in vivo stability of Bud23 and Mtq2, but not Nop2, Rcm1, or Trm11. Wild-type (AJY2643) or *trm112*Δ (AJY3517) cells expressing Bud23-13myc (pAJ2192), Nop2-13myc (pAJ2875), Rcm1-13myc (pAJ2878), Trm11-13myc (pAJ2876), or Mtq2-13myc (pAJ2877) from a plasmid were grown in selective media. Cells corresponding to 2.5 OD_{600} units from log-phase cultures were harvested and subjected to alkaline lysis followed by Western blotting. Myc-tagged proteins were detected using anti-myc antibody. Glucose-6-phosphate dehydrogenase (G6PDH) was detected as a control using anti-G6PDH antibody. (B) Overexpression of Trm112 stabilizes Bud23 in vivo. Wild-type cells (AJY2643) expressing plasmid-borne Bud23-GFP (pAJ2151) and galactose-inducible Trm112 (pAJ2583) or empty vector were grown overnight in selective media containing galactose at 30°C. Cultures were diluted in selective media containing galactose to OD_{600} ~ 0.1. Cells from log-phase cultures corresponding to 2.5 OD_{600} units were harvested after 6 and 24 h of growth. Cells were lysed by alkaline treatment, and proteins were detected by Western blotting. Bud23-GFP, Trm112-zz, and G6PDH were detected by anti-GFP, peroxidase-anti-peroxidase (PAP), and anti-G6PDH antibodies, respectively.

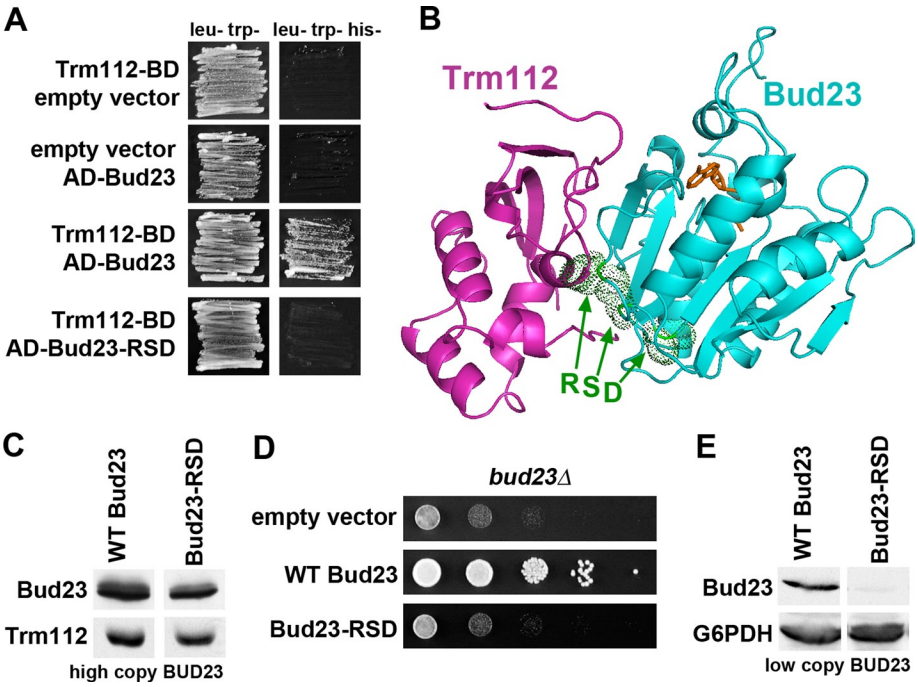

FIGURE 8: The Bud23-Trm112 interaction is biologically significant. (A) Specific mutations in Bud23 result in loss of Bud23-Trm112 two-hybrid interaction. PJ69-4α strain containing Trm112-Gal4BD (pAJ2895) and Gal4AD-Bud23 (pAJ2768) or Gal4AD-Bud23-RSD (pAJ2907) mutant on plasmids was patched on Leu-Trp and Leu-Trp-His plates. Corresponding controls (described in Figure 1B) were also patched in parallel. Plates were incubated at 30°C for 2 d. (B) Bud23 modeled structure (aa 1–219) manually docked into the recent *Encephalitozoon cuniculi* Trm112-Mtq2 structure (PDB 3Q87). Trm112 in magenta, Bud23 in cyan, SAM in orange, mutated residues in Bud23 (R107, S110 and D112) indicated as dotted spheres in green. (C) Loss of two-hybrid interaction is not explained by loss of protein levels. PJ69-4α strain containing Trm112-Gal4BD (pAJ2895) and Gal4AD-Bud23 (pAJ2768) or Gal4AD-Bud23-RSD (pAJ2907) on 2 μ (high-copy) plasmids used in Figure 7A was grown in Leu-Trp media. Cells corresponding to 2.5 OD_{600} units from log-phase cultures were subjected to alkaline lysis. Proteins were separated by SDS–PAGE and subjected to Western blotting. Gal4AD-hemagglutinin-Bud23 and Trm112-Gal4BD-myc were detected by anti-hemagglutinin (HA) and anti-myc antibodies, respectively. (D) Failure to interact with Trm112 results in loss of biological activity of Bud23. *bud23*Δ mutant (AJY2161) containing empty vector, wild-type Bud23 (pAJ2154), or Bud23-RSD mutant (pAJ2798) was assayed for function by growth complementation. Tenfold serial dilutions of normalized log-phase cultures were spotted on synthetic media lacking leucine. Plates were incubated at 30°C for 2 d. (E) Failure to interact with Trm112 results in reduced in vivo stability of Bud23. *bud23*Δ mutant (AJY2161) containing N-terminal myc-tagged wild-type Bud23 (pAJ2892) or Bud23-RSD mutant (pAJ2894) on low-copy plasmids was grown in selective media lacking leucine. Cells corresponding to 2.5 OD_{600} units from log-phase cultures were subjected to alkaline lysis. Proteins were separated by SDS–PAGE and subjected to Western blotting. myc-Bud23 was detected by anti-myc antibody. G6PDH was detected using anti-G6PDH antibody as a loading control.

position of the 90S pre-ribosomal particle. We have examined the sedimentation behavior of Trm112 and Bud23, using tagged versions of the proteins. We took advantage of the fact that the tags differentially affect the sedimentation of Bud23; Bud23 containing GAL4 binding domain fused to the N-terminus sediments at 90S, whereas it sediments at 40S with GFP fused to the C-terminus. Both fusion proteins are functional in vivo. Thus we could use these tagged Bud23 proteins to examine the dependence of Trm112 sedimentation on Bud23. We found that tagged Bud23 and Trm112 do not cosediment, and that Trm112 sedimentation is not affected by the presence or absence of Bud23. These results indicate that Trm112 and Bud23 are not maintained in a stable complex, despite the fact that the stability of Bud23 is dependent on the presence of Trm112. Together, these results suggest that transient interaction between Bud23 and Trm112 is sufficient for Bud23 stability. This could be explained if Trm112 stabilizes free Bud23 that is not engaged with substrate. Trm112 may also be important in delivering Bud23 to its substrate. Trm112 is reported to be expressed at 4800 molecules per cell, whereas Mtq2, Bud23, Trm9, and Trm11 combined are reported to be 8900 molecules per cell (Ghaemmaghami *et al.*, 2003). This is apart from additional Trm112 interactions with Dhr1 (Krogan *et al.*, 2006), Lys9 (Mazauric *et al.*, 2010), Sfh1 (Yu *et al.*, 2008), and Nop2 and Rcm1 identified here. Thus it seems unlikely that that there is sufficient Trm112 in a cell to bind all its partners simultaneously, consistent with the conclusion that Trm112 does not remain in a stable complex with Bud23. This may be a general property of how Trm112 interacts with its methyltransferase partners in the cellular context.

Trm112 interacts with multiple methyltransferases involved in various facets of ribosome function. However, *trm112*Δ and *bud23*Δ mutants show strong positive genetic interaction: the double mutant grows at essentially the same rate as the individual single mutants. This is consistent with the nearly total loss of Bud23 from cells lacking Trm112; if Bud23 is unstable in a *trm112*Δ mutant, deletion of BUD23 is not expected to worsen the phenotype. We modeled the predicted structure of Bud23 (White *et al.*, 2008; Figaro *et al.*, 2012) on the recent crystal structure of Mtq2-Trm112 (Liger *et al.*, 2011). We then mutated groups of adjacent surface-exposed residues and assayed for loss of interaction. Mutating the cluster of residues R107, S110, D112 resulted in loss of interaction with Trm112 and loss of function of Bud23. Although the mutant protein was expressed at close to wild-type levels when overexpressed in a two-hybrid construct, the protein was undetectable when expressed from a low-copy centromeric vector, consistent with our conclusion that Trm112 interaction is necessary for the maintenance of Bud23. Interestingly, Figaro *et al.* (2012) noted that the rid2-1 mutant in the *Arabidopsis* Bud23 homologue corresponds to position R107. rid2-1 is a partial loss-of-function mutant that displays rRNA-processing defects consistent with a defect in Bud23-like function (Ohbayashi *et al.*, 2011). Because R107 is in the cluster of residues affecting the interaction of Bud23 with Trm112 in yeast, it is likely that the rid2-1 mutant is specifically defective for interaction with *Arabidopsis* Trm112 homologue.

Extending the function of Trm112 to biogenesis of both ribosomal subunits

The fact that we could partially suppress the growth defect of a *trm112*Δ mutant with a utp14 mutation that we identified as a suppressor of *bud23*Δ suggests that a significant component of the growth defect of a *trm112*Δ mutant is due to the loss of Bud23. The

specific function of UTP14 in ribosome biogenesis is not known, and the mechanism of how utp14-A758G suppresses a *bud23Δ* mutant is something we are currently studying. Intriguingly, suppression of *trm112Δ* by a utp14 mutation revealed an underlying 60S biogenesis defect that was also evident in the underaccumulation of 25S rRNA in a *trm112Δ* mutant alone. These results indicate that Trm112 plays a role in 60S biogenesis in addition to its role in 40S biogenesis through Bud23. We found that Trm112-TAP sedimented primarily at the position of 60S and not 90S or pre-40S. This is consistent with Trm112 having a role in 60S biogenesis and its interaction with Nop2 and Rcm1 (reported here) and additional 60S factors (reported by Figaro *et al.*, 2012). Indeed, the enrichment for the pre-60S 27S and 7S RNAs with Trm112 strongly supports a role for Trm112 in 60S biogenesis. However, the sedimentation of Trm112-TAP at 60S is different than what was reported for native Trm112, which sedimented at 90S (Figaro *et al.*, 2012). Although we used TAP-tagged Trm112 in our experiments, this tagged version of Trm112 displays wild-type growth (unpublished data; Figaro *et al.*, 2012). Thus sedimentation at 60S suggests stable interaction with a 60S-related factor. Because Trm112 is a known partner for SAM-dependent methyltransferases or proteins containing the methyltransferase fold, we looked for interaction between Trm112 and known and putative methyltransferases implicated in 60S biogenesis by coimmunoprecipitation. We found Nop2 and Rcm1 as positive hits for interaction with Trm112. Interestingly, Nop2 was also identified in a recent Trm112-TAP purification (Figaro *et al.*, 2012). Nop2 is a nucleolar protein required for 27S pre-rRNA processing in 60S biogenesis (Hong *et al.*, 2001). It has been suggested to be a rRNA m5C methyltransferase (Pavlopoulou and Kossida, 2009; Petrossian and Clarke, 2009), but its activity and its modification site have not been characterized (Reid *et al.*, 1999; Hong *et al.*, 2001). Rcm1 (YNL022C) is also suggested to be an rRNA m5C methyltransferase closely related to Nop2 (Pavlopoulou and Kossida, 2009). However, like Nop2, its substrate is unknown. Thus it is of interest to identify the substrates for these putative methyltransferases to determine whether Trm112 is required for their methylation activities, as was recently demonstrated for Bud23-catalyzed methylation at position G1575 in 18S rRNA (White *et al.*, 2008; Figaro *et al.*, 2012).

MATERIALS AND METHODS

Strains, plasmids, and media

All yeast strains used in this study are listed in Table 1. Trm112-TAP–tagged and Utp14-GFP–tagged strains were obtained from Open Biosystems (Lafayette, CO; Ghaemmaghami *et al.*, 2003; Huh *et al.*, 2003). AJY3517 (*trm112Δ::G418r*) was obtained by sporulation and dissection of *TRM112/trm112Δ* heterozygous diploid strain from Open Biosystems (Winzeler *et al.*, 1999). AJY3524, AJY3549, AJY3547, AJY3538, and AJY3541 were generated by mating the corresponding parent strains, sporulated by patching on sporulation medium for 5–7 d at room temperature, and dissected on yeast–peptone–dextrose (YPD) medium. All strains were confirmed by growth on selection media and by PCR for the specific gene deletion or tag.

Cells were cultured at 30°C, unless otherwise indicated, in rich medium or synthetic dropout medium containing 2% glucose. All microbiological techniques and cloning were performed as previously described (Sambrook *et al.*, 1989). For quantification of Trm112-Bud23 genetic interaction, cells were cultured in 100 µl of YPD containing 75 µg/ml ampicillin in 96-well plates by shaking continuously for 36 h in a Powerwave microplate reader (Biotek, Winooski, VT). The doubling times were calculated from growth curves as previously described (Toussaint and Conconi, 2006).

All plasmids and oligos used in this study are listed in Tables 2 and 3, respectively. Details of plasmid construction are available upon request.

Two-hybrid interaction assay

For two-hybrid analysis, the indicated activation domain (AD) and binding domain (BD) plasmids (Louvet *et al.*, 1997) were transformed into PJ69-4α (James *et al.*, 1996) and selected on dropout media lacking leucine and tryptophan. The transformants were then

Strain	Genotype	Source
AJY3446	*MATa Trm112-GFP::HIS3MX6 leu2Δ0 ura3Δ0*	Huh *et al.*, 2003
PJ69-4α	*MATα trp1-901 leu2-3112 ura3-52 his3Δ200 gal4Δ gal80Δ LYS2::GAL1-HIS3 GAL2-ADE met2::GAL7-LACZ*	James *et al.*, 1996
AJY2643	*MATa his3Δ1 leu2Δ0 met15Δ0 ura3Δ0*	Winzeler *et al.*, 1999
AJY3517	*MATα trm112Δ::G418r his3Δ1 leu2Δ0 ura3Δ0*	This study
AJY2676	*MATa bud23Δ::Natr his3Δ1 leu2Δ0 ura3Δ0*	This study
AJY2161	*MATa bud23Δ::G418r his3Δ1 leu2Δ0 ura3Δ0 lys2Δ0 met15Δ0*	White *et al.*, 2008
AJY3524	*MATa trm112Δ::G418r bud23Δ::G4184 his3Δ1 leu2Δ0 ura3Δ0*	This study
AJY3549	*MATa bud23Δ::Natr4 utp14 A758G his3Δ1 leu2Δ0 ura3Δ0*	This study
AJY3547	*MATα trm112Δ::G418r utp14 A758G his3Δ1 leu2Δ0 ura3Δ0*	This study
AJY3261	*MATa Utp14-GFP::HIS3MX6 leu2Δ0 ura3Δ0*	Huh *et al.*, 2003
AJY3538	*MATa Utp14-GFP::HIS3MX6 trm112Δ::G418r leu2Δ0 ura3Δ0*	This study
AJY3263	*MATa Utp14-GFP::HIS3MX6 bud23Δ::G418r leu2Δ0 ura3Δ0*	This study
AJY3541	*MATα utp14 A758G-GFP::HIS3MX6 trm112Δ::G418r leu2Δ0 ura3Δ0*	This study
AJY3262	*MATa utp14A758G-GFP::HIS3MX6 bud23Δ::Natr leu2Δ0 ura3Δ0*	This study
AJY3560	*MATa Trm112-TAP::HIS3MX6 leu2Δ0 ura3Δ0*	Ghaemmaghami *et al.*, 2003
AJY3125	*MATa Trm112-TAP::HIS3MX6 bud23Δ::G418r leu2Δ0 ura3Δ0*	This study

TABLE 1: Strains used in this study.

pAJ	Description	Source
2558	*BUD23-TAP LEU2 CEN ARS*	This study
2151	*BUD23-GFP LEU2 CEN ARS*	This study
2895	*TRM112-GAL4BD-cmyc TRP1 2* μ	This study
2768	*GAL4AD-HA-BUD23 LEU2 2* μ	This study
2907	*Gal4AD-HA-bud23-RSD LEU2 2* μ	This study
2351	*pGBKT7 TRP1 2* μ	Louvet *et al.*, 1997
2144	*pACT2 LEU2 2* μ	Clontech
2192	*BUD23-13myc LEU2 CEN ARS*	This study
2875	*NOP2-13myc LEU2 CEN ARS*	This study
2878	*RCM1-13myc LEU2 CEN ARS*	This study
2876	*TRM11-13myc LEU2 CEN ARS*	This study
2877	*MTQ2-13myc LEU2 CEN ARS*	This study
2583	*pGAL1-TRM112-zz-6XHIS URA3*	Gelperin *et al.*, 2005
2154	*BUD23 LEU2 CEN ARS*	White *et al.*, 2008
2798	*BUD23-RSD LEU2 CEN ARS*	This study
2872	*RRP8-13myc URA3 CEN ARS*	This study
2873	*YBR141C-13myc URA3 CEN ARS*	This study
2874	*YBR063W-13myc URA3 CEN ARS*	This study
2879	*YBR271W-13myc URA3 CEN ARS*	This study
2890	*SPB1-13myc URA3 CEN ARS*	This study
2892	*GAL4BD-myc-BUD23 LEU2 CEN ARS*	This study
2894	*GAL4BD-myc-BUD23-RSD LEU2 CEN ARS*	This study

TABLE 2: Plasmids used in this study.

patched on dropout media lacking leucine, tryptophan, and histidine to test for two-hybrid interaction.

Immunoprecipitation and Western blotting

For immunoprecipitations, cultures were grown to an OD_{600} of 0.6–0.8 in selective medium. Cells were resuspended in IP buffer (100 mM NaCl, 50 mM Tris-HCl, pH 7.5, 1.5 mM $MgCl_2$, 0.15% NP40, 1 mM phenylmethylsulfonyl fluoride (PMSF), 1 μg/ml leupeptin, 1 μg/ml pepstatin A), lysed by vortexing with glass beads, and clarified by centrifugation at 15,000 × *g* at 4°C. Immunoprecipitation was performed for the protein A tag by incubating extracts with IgG-Sepharose beads (IgG Sepharose 6 Fast Flow; Amersham, Pittsburgh, PA) for 1 h at 4°C; this was followed by tobacco etch virus protease (TEV) enzyme cleavage at 16°C for 2 h. The beads were separated from the TEV eluate by centrifugation at 2000 × *g* for 30 s. The eluted proteins were precipitated by adding 10% TCA. For Northern blotting from immunoprecipitated samples, TEV eluates were subjected to acid phenol:chloroform extraction as previously described (Sambrook *et al.*, 1989). The RNA in the aqueous phase was precipitated with 2.5 vol ethanol and 0.1 vol sodium acetate (pH 5) at –20°C for 24 h. Proteins in the organic phase were precipitated with 2 vol acetone at –20°C for 24 h.

For Western blotting, membranes were incubated with the appropriate primary antibody for 2 h at room temperature or overnight at 4°C and with the secondary antibody for 30 min at room temperature.

AJO	Target	Sequence
603	35S	TGTTACCTCTGGGCCCCGATTG
603	27SA2	TGTTACCTCTGGGCCCCGATTG
282	27S, 7S	GGCCAGCAATTTCAAGTTA
130	20S	TCTTGCCCAGTAAAAGCTCTCATGC
190	18S	GTCTGGACCTGGTGAGTTTCCC
192	25S	CCCGCCGTTTACCCGCGCTTGG
603	23S	TGTTACCTCTGGGCCCCGATTG
962	U2	GCGACCAAAGTAAAAGTCAAGAAC-GACTCCACAAGTGCGAGGGTCGCGAC
1686	U3	TAGATTCAATTTCGGTTTCTC

TABLE 3: Oligos used in this study.

Microscopy

Overnight cultures were diluted to an OD_{600} of 0.1 into fresh selective medium and allowed to grow for 4–5 h at 30°C. Fluorescence was visualized on a Nikon (Melville, NY) E800 microscope fitted with a Plan Apo 100×/1.4 objective and a Photometrics CoolSNAP ES camera (Tucson, AZ) controlled by NIS-Elements AR version 2.10 software. Images were prepared using Adobe Photoshop CS5 (San Jose, CA).

Sucrose density gradient sedimentation

For polysome profile analysis, cells were grown at 30°C to an OD_{600} of 0.3. Cycloheximide (100 μg/ml) was added to the cultures; this was followed by incubation in the 30°C shaker for 10 min. The cells were then immediately poured onto ice and collected by centrifugation. All steps were carried out at 0–4°C. Cells were washed with lysis buffer (100 mM KCl, 50 mM Tris-HCl, pH 7.5, 5 mM $MgCl_2$, 150 μg/ml cycloheximide, 7 mM beta-mercaptoethanol [BME], 1 mM PMSF, 1 μg/ml leupeptin, 1 μg/ml pepstatin A) and lysed by vortexing in the presence of glass beads. For dissociative gradients, cells were not treated with cycloheximide before harvesting, and extracts were prepared in lysis buffer lacking cycloheximide and magnesium. Extracts were centrifuged for 10 min at 15,000 × *g* at 4°C, and 9 OD_{260} units of clarified extract were loaded onto 7–47% sucrose gradients prepared in the appropriate buffer and centrifuged for 2.5 h at 40,000 rpm (SW40 rotor; Beckman). Gradients were fractionated (Model 640; ISCO, Lincoln, NE) with continuous monitoring at 254 nm. Fractions were precipitated with 10% TCA overnight at –20°C. The pellets were resuspended in Laemmli buffer and boiled at 99°C for 5 min. Proteins were separated on 8% SDS–PAGE gels, transferred to a nitrocellulose membrane, and subjected to Western blot analysis.

Northern blotting

All RNAs were prepared using acid phenol:chloroform extraction as previously described (Sambrook *et al.*, 1989). RNAs were separated by 1% agarose-formaldehyde gel electrophoresis and transferred to Zeta-Probe GT membrane (Bio-Rad, Hercules, CA) by capillary transfer. The transferred RNAs were UV cross-linked to the membrane, and Northern blotting, using 5′-[^{32}P]-labeled oligonucleotide probes, was performed as described previously (Li *et al.*, 2009). The hybridization signals were detected by phosphorimaging and quantified using Quantity One (Bio-Rad).

ACKNOWLEDGMENTS

We thank S. Baserga for anti-Mpp10, G Dieci for anti-Rps8, and Z Li for plasmids and mass spectroscopy support. This work was supported by a National Institutes of Health grant (GM53655) to A.W.J.

REFERENCES

Chen C, Huang B, Anderson JT, Bystrom AS (2011). Unexpected accumulation of ncm(5)U and ncm(5)S(2) (U) in a trm9 mutant suggests an additional step in the synthesis of mcm(5)U and mcm(5)S(2)U. PloS One 6, e20783.

Decatur WA, Fournier MJ (2002). rRNA modifications and ribosome function. Trends Biochem Sci 27, 344–351.

Dixon SJ, Costanzo M, Baryshnikova A, Andrews B, Boone C (2009). Systematic mapping of genetic interaction networks. Annu Rev Genet 43, 601–625.

Dunin-Horkawicz S, Czerwoniec A, Gajda MJ, Feder M, Grosjean H, Bujnicki JM (2006). MODOMICS: a database of RNA modification pathways. Nucleic Acids Res 34, D145–D149.

Figaro S, Wacheul L, Schillewaert S, Graille M, Huvelle E, Mongeard R, Zorbas C, Lafontaine DL, Heurgue-Hamard V (2012). Trm112 is required for Bud23-mediated methylation of the 18S rRNA at position G1575. Mol Cell Biol 32, 2254–2267.

Gelperin DM *et al.* (2005). Biochemical and genetic analysis of the yeast proteome with a movable ORF collection. Genes Dev 19, 2816–2826.

Ghaemmaghami S, Huh WK, Bower K, Howson RW, Belle A, Dephoure N, O'Shea EK, Weissman JS (2003). Global analysis of protein expression in yeast. Nature 425, 737–741.

Helm M (2006). Post-transcriptional nucleotide modification and alternative folding of RNA. Nucleic Acids Res 34, 721–733.

Henras AK, Soudet J, Gerus M, Lebaron S, Caizergues-Ferrer M, Mougin A, Henry Y (2008). The post-transcriptional steps of eukaryotic ribosome biogenesis. Cell Mol Life Sci 65, 2334–2359.

Heurgue-Hamard V, Graille M, Scrima N, Ulryck N, Champ S, van Tilbeurgh H, Buckingham RH (2006). The zinc finger protein Ynr046w is plurifunctional and a component of the eRF1 methyltransferase in yeast. J Biol Chem 281, 36140–36148.

Hong B, Wu K, Brockenbrough JS, Wu P, Aris JP (2001). Temperature sensitive nop2 alleles defective in synthesis of 25S rRNA and large ribosomal subunits in *Saccharomyces cerevisiae*. Nucleic Acids Res 29, 2927–2937.

Huh WK, Falvo JV, Gerke LC, Carroll AS, Howson RW, Weissman JS, O'Shea EK (2003). Global analysis of protein localization in budding yeast. Nature 425, 686–691.

James P, Halladay J, Craig EA (1996). Genomic libraries and a host strain designed for highly efficient two-hybrid selection in yeast. Genetics 144, 1425–1436.

Krogan NJ *et al.* (2006). Global landscape of protein complexes in the yeast *Saccharomyces cerevisiae*. Nature 440, 637–643.

Lafontaine D, Delcour J, Glasser AL, Desgres J, Vandenhaute J (1994). The DIM1 gene responsible for the conserved m6(2)Am6(2)A dimethylation in the 3′-terminal loop of 18 S rRNA is essential in yeast. J Mol Biol 241, 492–497.

Lafontaine D, Vandenhaute J, Tollervey D (1995). The 18S rRNA dimethylase Dim1p is required for pre-ribosomal RNA processing in yeast. Genes Dev 9, 2470–2481.

Li Z, Lee I, Moradi E, Hung NJ, Johnson AW, Marcotte EM (2009). Rational extension of the ribosome biogenesis pathway using network-guided genetics. PLoS Biol 7, e1000213.

Liger D, Mora L, Lazar N, Figaro S, Henri J, Scrima N, Buckingham RH, van Tilbeurgh H, Heurgue-Hamard V, Graille M (2011). Mechanism of activation of methyltransferases involved in translation by the Trm112 "hub" protein. Nucleic Acids Res 39, 6249–6259.

Louvet O, Doignon F, Crouzet M (1997). Stable DNA-binding yeast vector allowing high-bait expression for use in the two-hybrid system. Biotechniques 23, 816–818, 820.

Mazauric MH, Dirick L, Purushothaman SK, Bjork GR, Lapeyre B (2010). Trm112p is a 15-kDa zinc finger protein essential for the activity of two tRNA and one protein methyltransferases in yeast. J Biol Chem 285, 18505–18515.

Ohbayashi I, Konishi M, Ebine K, Sugiyama M (2011). Genetic identification of Arabidopsis RID2 as an essential factor involved in pre-rRNA processing. Plant J 67, 49–60.

Pavlopoulou A, Kossida S (2009). Phylogenetic analysis of the eukaryotic RNA (cytosine-5)-methyltransferases. Genomics 93, 350–357.

Petrossian TC, Clarke SG (2009). Multiple Motif Scanning to identify methyltransferases from the yeast proteome. Mol Cell Proteomics 8, 1516–1526.

Piekna-Przybylska D, Decatur WA, Fournier MJ (2007). New bioinformatic tools for analysis of nucleotide modifications in eukaryotic rRNA. RNA 13, 305–312.

Purushothaman SK, Bujnicki JM, Grosjean H, Lapeyre B (2005). Trm11p and Trm112p are both required for the formation of 2-methylguanosine at position 10 in yeast tRNA. Mol Cell Biol 25, 4359–4370.

Reid R, Greene PJ, Santi DV (1999). Exposition of a family of RNA m(5)C methyltransferases from searching genomic and proteomic sequences. Nucleic Acids Res 27, 3138–3145.

Sambrook J, Fritsch EF, Maniatis T (1989). Molecular Cloning: A Laboratory Manual, Cold Spring Harbor, NY: Cold Spring Harbor Laboratory Press.

Studte P, Zink S, Jablonowski D, Bar C, von der Haar T, Tuite MF, Schaffrath R (2008). tRNA and protein methylase complexes mediate zymocin toxicity in yeast. Mol Microbiol 69, 1266–1277.

Toussaint M, Conconi A (2006). High-throughput and sensitive assay to measure yeast cell growth: a bench protocol for testing genotoxic agents. Nature Protocols 1, 1922–1928.

White J, Li Z, Sardana R, Bujnicki JM, Marcotte EM, Johnson AW (2008). Bud23 methylates G1575 of 18S rRNA and is required for efficient nuclear export of pre-40S subunits. Mol Cell Biol 28, 3151–3161.

Winzeler EA *et al.* (1999). Functional characterization of the *S. cerevisiae* genome by gene deletion and parallel analysis. Science 285, 901–906.

Yu H *et al.* (2008). High-quality binary protein interaction map of the yeast interactome network. Science 322, 104–110.